2024 IEEE/RSJ International Conference on Intelligent Robots and Systems (IROS)
October 14-18, 2024. Abu Dhabi, UAE

Design and Control of a Novel Soft-Rigid Lower Limb Exoskeleton Robot

Yuxuan Wang[1], Shaoke Yuan[1], Zihan Pu[1], Jiangbei Wang[1], Yanqiong Fei[1,2,3]

Abstract— **This paper presents a study on the design and control of a novel soft-rigid lower limb exoskeleton robot. First, based on anatomy, a novel exoskeleton structure design is proposed that applies Curl Pneumatic Artificial Muscles (CPAMs) to lower limb joints to actuate lower limb movement, and transmit force and motion through rigid parts. A phenomenological characteristic model of the CPAM based on experimental tests and fitting methods is constructed for exoskeleton control. Then, a feedforward-feedback hybrid control method based on four CPAM characteristic models is proposed to improve the control accuracy and stability of the exoskeleton. A human-in-the-loop control method based on human-robot hybrid dynamics modeling and human intentions and states is proposed to improve the human-robot interaction performance of exoskeletons. Experimental results show that feedforward-feedback hybrid control can reduce the maximum tracking error of the exoskeleton to 3.4% for hip, 2.9% for knee, and 4.7% for ankle joint. The exoskeleton can achieve intentional control based on EMG signals. With the assistance of the exoskeleton, the muscle activity of the human lower limbs is reduced by an average of 32.2%. The proposed soft-rigid lower limb exoskeleton robot has the advantages of being lightweight, having good flexibility, being comfortable wearing and having good human-computer interaction, which can improve efficiency. In the future, it will provide more effective intelligent rehabilitation equipment for patients with lower limb movement disorders.**

I. Introduction

Rehabilitation robots can reduce the burden on therapists, realize data detection during training, assist rehabilitation in a controllable and repeatable manner, and complete quantitative evaluation of rehabilitation effects at the same time, which has broad application prospects in rehabilitation therapy. Exoskeleton rehabilitation robots are representative of rehabilitation robots [1]. At present, exoskeleton rehabilitation robots have been widely researched and developed to assist the movement of various joints in human body [2]–[4].

Exoskeleton rehabilitation robots can be divided into three categories according to their stiffness, driving methods and power transmission methods: rigid exoskeleton rehabilitation robots, soft exoskeleton rehabilitation robots, and soft-rigid exoskeleton rehabilitation robots. Rigid exoskeleton rehabilitation robots have advantages including the stability of the rigid structure, providing sufficient support, and achieving precise force transmission [5]. Some companies have developed a series of rigid exoskeleton rehabilitation robots, such as Parker Hannifin's Indego [6], ATLAS 2020 developed by the Spanish National Research Council [7], etc. However, they have problems such as high quality, poor user experience, and poor security. Tiana et al. [8] composed a soft pneumatic exoskeleton proposed for hip flexion rehabilitation. Liu et al. [9] designed a new flexible ankle rehabilitation robot. However, they have problems such as insufficient support, low integration, and difficulty in control. In terms of control, the current soft exoskeleton robots don't have quick response and good user interaction [10], [11], which means there is a mismatch between the user's movements and the robot's actions. This stops users from fully benefitting from the robot's abilities to improve their movement. Therefore, exoskeleton robots need to be designed with the user in mind, and including human elements in the control process is crucial for the robot to be effective.

In this paper, we proposed a novel soft-rigid lower limb exoskeleton robot and the main contributions of this paper are as follows: (1) Based on anatomy, a novel exoskeleton structure design is proposed that applies Curl Pneumatic Artificial Muscles (CPAMs) to lower limb joints to actuate lower limb movement, and transmit force and motion through rigid parts. (2) A feedforward-feedback hybrid control method based on four CPAM characteristic models is proposed to improve the control accuracy and stability of the exoskeleton. (3) A human-in-the-loop control method based on human-robot hybrid dynamics modeling and human intentions and states is proposed to improve the human-robot interaction performance of exoskeletons.

II. Design

In anatomy, the lower limb of human body mainly includes three joints (hip, knee, and ankle) and three skeletal regions (thigh, crus, and foot), in which the hip joint links the whole lower limb to the waist. Besides the flexion/extension in the sagittal plane, each biological joint has additional DOFs, such as the lateral/medial rotation and abduction/adduction of the hip, the lateral/medial rotation of the knee, and the inversion/eversion of the ankle. Coordinated motion of these multi-DOF joints ensures the effectiveness and stability of the normal walk. In the design of exoskeletons, only the DOFs significantly contributing to the power of walking are considered, that is, the flexion/extension within the sagittal plane, for reducing the complexity and weight of the exoskeleton.

This work was supported by National Key tech nologies research and development program of China under Grant No.2022YFB4703202, National Facility of Translational Medicine (Shanghai) under Grant No.TMSK2021-110, Institute of Medical Robotics of Shanghai Jiao Tong University under Grant No.IMR2019KY01. (*Corresponding author: Yanqiong Fei.*)

[1]Research Institute of Robotics, [2]Institute of Medical Robotics, [3]ShenZhen Research Institute, Shanghai Jiao Tong University. (E-mail: {wangyx_23, yuanshaoke, puzihan2000, J.B.Wang}@sjtu.edu.cn, fyq_sjtu@163.com.)

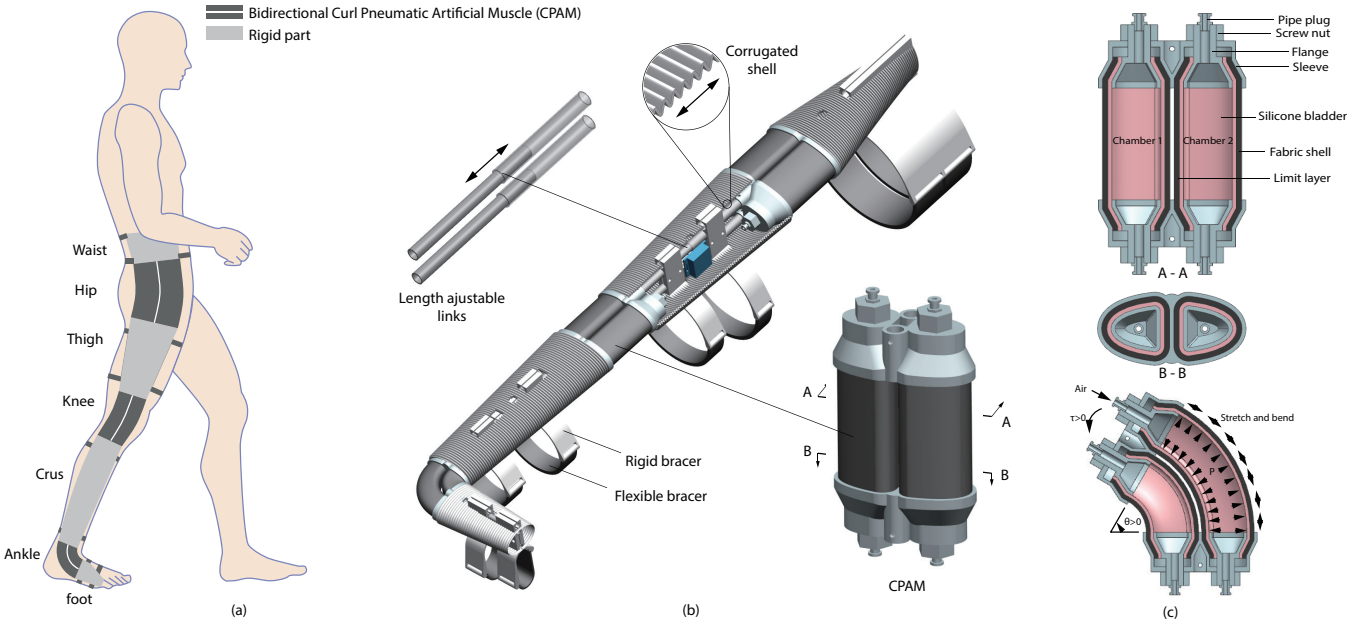

Fig. 1. Design of the soft-rigid exoskeleton. (a) The soft-rigid exoskeleton weared on human. (b) The structure of soft-rigid exoskeleton. (c) The structure of bidirectional CPAM.

A. *Exoskeleton Structure*

The proposed soft-rigid exoskeleton is designed to assist the flexion and extension of the hip, knee, and ankle joints through three customized bidirectional CPAMs, which are connected by four rigid parts corresponding to the waist, thigh, crus, and foot, respectively (Fig.1(a)).

Within each rigid part, a pair of length adjustable links (made of carbon fiber tubes) are utilized as the connector between proximal and distal CPAMs, and the flexible corrugated shell (3D-printed by thermoplastic polyurethane) can stretch in response to length variation of the links(Fig.1b). This design allows the exoskeleton to be adapted for users of different heights. On the links, two rigid bracers (3D-printed by nylon powder) are attached, which supply the human-exoskeleton interface as well as complete the force transfer from exoskeleton to human body. The flexible bracers (made of nylon fabric) ensure the rigid bracers to be worn on lower limb tightly.

The bidirectional CPAM mainly consists of two semi-elliptical cylindrical air chambers (Fig.1c). Relevant research on pneumatic soft actuators [12], [13] indicates that modifying the cross-sectional shape of these actuators can boost the cross-sectional static moment for a given area, thus enhancing the actuating torque. Therefore, CPAMs adopted an elliptical cross-section, decreasing the width and the height of the cross-section. Each chamber is composed of a silicone bladder (made of ELASTOSIL M 4601 A/B), a longitudinally elastic fabric shell (made of rubber-blended polyester-knitted fabric) and an inextensible limit layer (made of polyvinyl chloride coated polyester woven fabric). The flange and sleeve (made of aluminum alloy by machining) with conic surface are used to clamp two ends of the bladder, shell and limit layer, thus sealing up the air chamber, where the tightness is adjusted by the screw nut. We believe that CPAMs have flexibility and adaptability, which can automatically adapt to the axis change in the rotation of human joints, compensate the offset and dislocation between CPAMs and human joints, and be safer in the process of assisting the movement of human lower limbs.

Air can be pumped into the chambers through the pipe plug to make the CPAM bend (Fig.1c) and thus drive the physical joint of lower limb to rotate. Pressurization of the chamber on one side leads to the bending deformation toward another side, and thus the bidirectional bending can be achieved. The bending deformation is generated because the fabric shell on the pressurized side stretches while the limit layer keeps inextensible. The inflating pressure (P), the bending angle (θ) and the produced torque (τ) are related with each other, which will be explored in the next section.

The proposed soft-rigid exoskeleton has total weight of no more than $5\,\mathrm{kg}$ per leg by using multiple lightweight materials including carbon fiber, aluminum, thermoplastic polyurethane, nylon, silicone and fabrics. Therefore, the proposed exoskeleton has advantages of low gravity load and small inertia effect on human body compared with fully rigid exoskeletons.

B. *Actuator characteristic*

According to the law of conservation of energy, the inflating pressure produces bending motion and output torque. Therefore the actuating torque (τ) is related to the inflating pressure (P) and the bending angle (θ). The pressure-angle-torque relationship can provide the characteristic model for feedforward control. The characteristic of the actuator can be denoted by Eq.(1).

$$\tau = f(P, \theta) \tag{1}$$

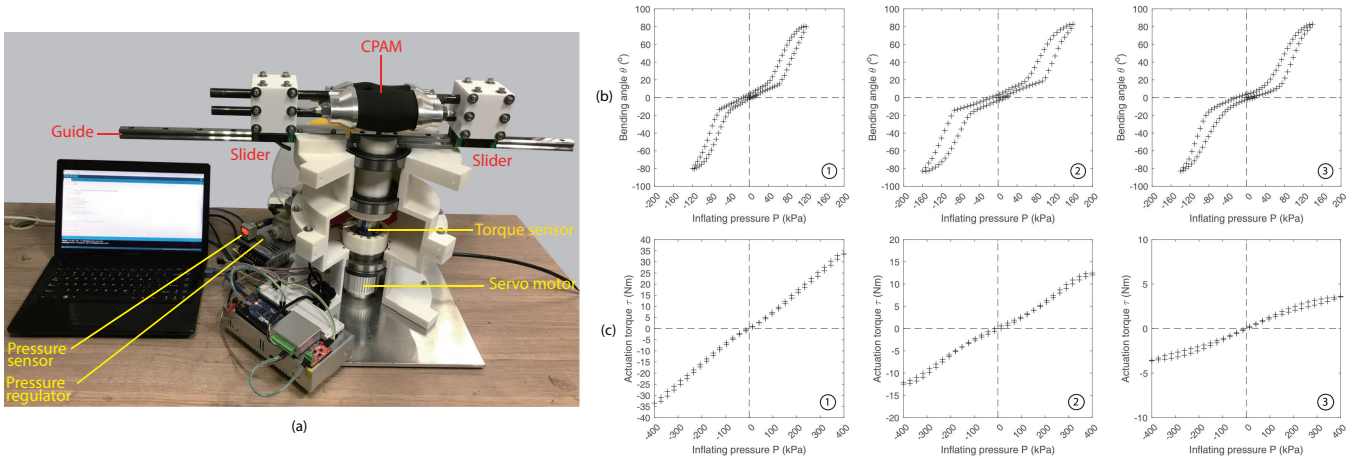

Fig. 2. Actuator characteristic experiment. (a) The experiment setup. (b) The measured pressure-angle data of ① CPAM for hip, ② CPAM for knee, ③ CPAM for ankle. (c) The measured pressure-torque data of ① CPAM for hip, ② CPAM for knee, ③ CPAM for ankle.

To determine the specific expression of Eq.(1), we test the bidirectional CPAM with different inflating pressures and bending angles, then measure the actuating torques, and finally fit the data by a bivariate function. Fig.2(a) shows the experiment setup, in which the inflating pressure, the bending angle and the actuating torque are measured by the pressure sensor, the angular encoder of the servo motor and the torque sensor respectively. Fig.2(b), (c) shows the measured data of pressure-angle and pressure-torque. It is observed that the bending angle increases monotonically and in an odd symmetrical, piecewise linear manner with the inflating pressure, while the actuating torque increases almost linearly with the inflating pressure. In our previous research [14], the relationship between the actuator's torque, angle, and air pressure is as shown in Eq.(2).

$$\tau = c[P - P_{\tau=0}(\theta)] \tag{2}$$

where c is the mean slope of the fitting line of pressure and torque and $P_{\tau=0}(\theta)$ is the piecewise function of pressure and angle.

It can be seen that the actuating torque increases when the inflating pressure increases or the bending angle decreases. The maximum actuating torques of $34.1\,\mathrm{N\,m}$ (hip), $12.5\,\mathrm{N\,m}$ (knee), $3.6\,\mathrm{N\,m}$ (ankle) are reached when the CPAM is inflated by a maximum pressure of $400\,\mathrm{kPa}$ with zero bending angle. In rehabilitation, the limb moves very slowly and can be considered a quasi-static process. The static torque range of normal human joints are: -60-50 $\mathrm{N\,m}$ (hip), -10-25 $\mathrm{N\,m}$ (knee) and -20-25 $\mathrm{N\,m}$ (ankle) [15], so the torque provided by the exoskeleton can meet the needs of low-intensity rehabilitation training. The maximum bending angles of $80.2°$ (hip), $82.7°$ (knee), $82.7°$ (ankle) are reached when the CPAM is inflated by a pressure of $200\,\mathrm{kPa}$ with zero actuating torque. According to Rehabilitation Medicine (Sixth Edition, People's Health Publishing House), the bending angles are compatible with the required range of lower limb joint motion for rehabilitation.

The significant negative correlation between the actuating torque and the inflating pressure indicates the property of low stiffness (Eq.(3)) or high compliance of the CPAM. The stiffness of the CPAM varies with the inflating pressure, and if the pressure is high, the stiffness is also high. Under the inflating pressure of $400\,\mathrm{kPa}$, the stiffness can reach $0.13\,\mathrm{N\,m/°}$ for hip, $0.06\,\mathrm{N\,m/°}$ for knee and $0.02\,\mathrm{N\,m/°}$ for ankle, lower than the lower limb's passive stiffness of human body. This low stiffness property ensures better operating safety and wearing comfortability of the proposed exoskeleton in interaction with human body compared to traditional rigid exoskeletons.

$$k = \frac{\partial \tau}{\partial \theta} \tag{3}$$

III. Method

This section proposes two control methods: feedforward-feedback hybrid control and human-in-the-loop control, with the aim of improving the control accuracy, stability and human-machine interaction performance of the exoskeleton.

A. Feedforward-feedback hybrid control

For soft actuators, due to the existence of effects such as gravity and hysteresis, feedback closed-loop control can't guarantee real-time control. Therefore, we add a model-based feedforward control unit to feedback closed-loop control to reduce the impact of gravity and hysteresis effect. To achieve feedforward and feedback control of exoskeleton, the entire control diagram includes feedforward control, feedback control, pressure control, and exoskeleton, shown in Fig.3(a). Feedforward control compensates for joint load torques caused by gravity and time delays caused by hysteresis to enhance control precision and stability. Feedback control further improves control accuracy on the basis of feedforward control.

Feedforward control (Fig.3(b)) refers to four models: pseudo-rigid body model, finite element model, phenomenological characteristic model, and hysteresis model. Based on the pseudo-rigid body model, it calculates the joint load torque (τ_{hd}, τ_{kd}, τ_{ad}) caused by gravity according to the

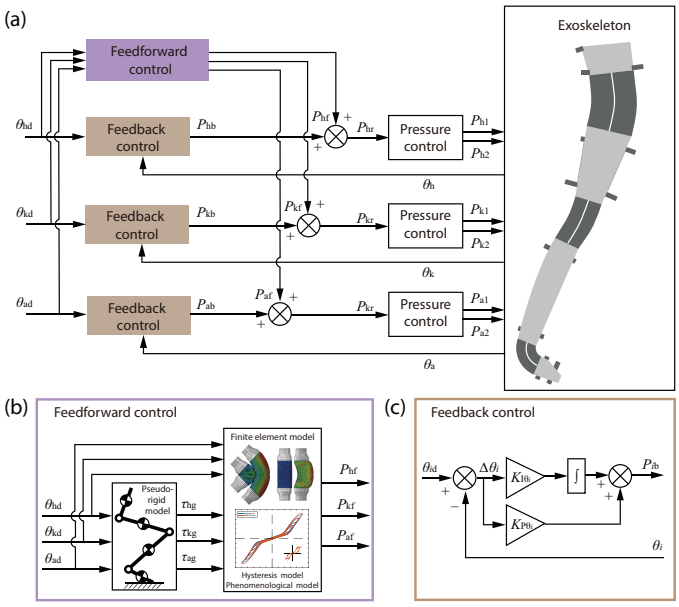

Fig. 3. Feedforward-feedback hybrid control. (a) General control scheme. (b) Feedforward control. (c) Feedback control.

target joint angles (θ_{hd}, θ_{kd}, θ_{ad}). Then, based on the finite element model [16], phenomenological characteristic model and hysteresis model of the CPAM, the relationship between CPAM inflation pressure, bending angle, and actuation torque is derived. According to the aforementioned target joint angle and joint load torque, the required inflation pressure (P_{hd}, P_{kd}, P_{ad}) for each joint of the exoskeleton is calculated. This is the feedforward inflation pressure needed for gravity compensation.

Feedback control (Fig.3(c)) first calculates the deviation ($\Delta\theta_i$) between the actual bending angles (θ_h, θ_k, θ_a) and the target bending angles (θ_{id}) of the exoskeleton joint. Then, a Proportional-Integral (PI) controller generates feedback inflation pressure (P_{ib}), as shown in Eq.(4) and Eq.(5).

$$\Delta\theta_i = \theta_{id} - \theta_i \tag{4}$$

$$P_{ib} = K_{P\theta i}\Delta\theta_i + K_{I\theta i}\int \Delta\theta_i dt \tag{5}$$

$K_{P\theta i}$ and $K_{I\theta i}$ represent the proportional and integral gains of the joint angle feedback control, respectively, where i=h,k,a denotes the hip, knee, and ankle joints. The feedback inflation pressure (P_{ib}) is implemented through pressure control and applied to the soft joints, thereby actuating the exoskeleton joints to produce bending movements according to the target signal. The proportional and integral gains are adjusted using the Good Gain method [17].

B. Human-in-the-loop control

The human-in-the-loop control method can make the exoskeleton robot a human-centered system and improve the effectiveness of the robot. The control method described in this section proposes a human-robot hybrid dynamics modeling method, which takes into account not only the characteristics of the robot, but also the user's status and active intention in the control system. The entire control diagram is shown in Fig.4.

The human-exoskeleton system receives signals of the inflating pressures (P_{h1}, P_{h2}, P_{k1}, P_{k2}, P_{a1}, P_{a2}) and output signals including the attitude angles of body segments (φ_b, φ_t, φ_c, φ_f), the actual bending angles of lower limb joints (θ_h, θ_k, θ_a) and the contact forces with ground (F_n, F_t). The inflating pressures are output from proportional valves. The attitude angles of body segments are monitored by the Inertial Measurement Units (IMUs). The bending angles of lower limb joints is obtained from the attitude angles according to Eq.(6). The contact forces with ground are measured by a triaxial load cell.

$$\begin{cases} \theta_h = \varphi_t - \varphi_b \\ \theta_k = \varphi_t - \varphi_c \\ \theta_a = \varphi_f - \varphi_c \end{cases} \tag{6}$$

Through statics analysis (shown in Fig.4 and Eq.(7)), we obtain the load torques ($\tau_h|_{load}$, $\tau_k|_{load}$, $\tau_a|_{load}$) acting on the lower limb joints, in which the gravity and contact forces are considered. The expression of load torques is with respect to the attitude angles of lower limb segments and the ground contact forces, and is also related with the mass, length and center of mass of lower limb segments listed in Table I.

$$\begin{cases} \tau_a|_{load} = m_f g S_f sin\varphi_f - F_n L_f sin\varphi_f + F_t L_f cos\varphi_f \\ \tau_k|_{load} = -\tau_a|_{load} - m_c g S_c sin\varphi_c \\ \qquad\qquad +(F_n - m_f g)L_c sin\varphi_c - F_t L_c cos\varphi_c \\ \tau_h|_{load} = -\tau_k|_{load} - m_t g S_t sin\varphi_t \\ \qquad\qquad -(F_n - m_f g - m_c g)L_t sin\varphi_t - F_t L_c cos\varphi_t \end{cases} \tag{7}$$

The bending motion of physical joints is retarded by a passive torque which is produced by the extension force of muscles. Due to existence of bi-articular muscles, the passive joint torque is influenced by the angular positions of adjacent joints. For instance, the passive torque of the knee joint depends on the knee angle as well as the hip and ankle angles. Riener [15] et al derived a double-exponential model to estimate the passive torques of lower limb joints of a 'generic subject', as expressed by Eq.(8). The tradition of joint angles and torques used by Riener et al is a little different from ours, and Eq.(9) presents the transformation between them.

$$\begin{cases} \tau'_h|_{passive} = e^{1.4655-0.0034\theta_k-0.0750\theta_h} \\ \qquad\qquad -e^{1.3403-0.0226\theta_k+0.0305\theta_h} + 8.072 \\ \tau'_k|_{passive} = e^{1.800-0.0460\theta'_a-0.0352\theta_k+0.0217\theta_h} \\ \qquad\qquad -e^{-3.971-0.0004\theta'_a+0.0495\theta_k-0.0128\theta_h} \\ \qquad\qquad -4.820 + e^{2.220-0.150\theta_k} \\ \tau_a|_{passive} = e^{2.1016-0.0843\theta'_a-0.0176\theta_k} \\ \qquad\qquad -e^{-7.9763+0.1949\theta'_a+0.0008\theta_k} - 1.792 \end{cases} \tag{8}$$

$$\begin{cases} \tau_h|_{passive} = -\tau'_h|_{passive} \\ \tau_k|_{passive} = -\tau'_k|_{passive} \\ \theta_a = 90^\circ - \theta'_a \end{cases} \tag{9}$$

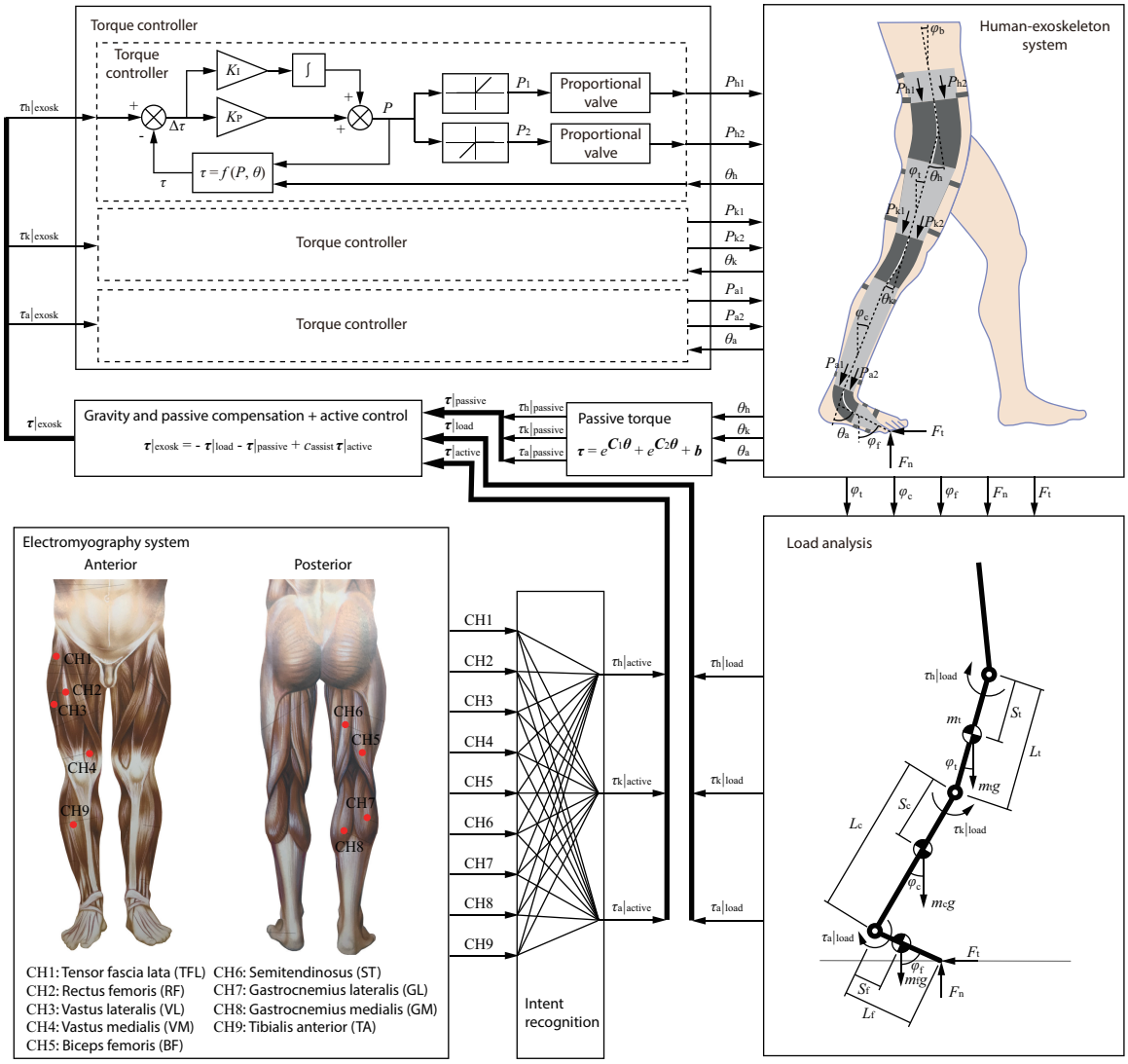

Fig. 4. The Human-in-the-loop control method based on the human-machine hybrid dynamics modeling of the exoskeleton robot.

TABLE I

PARAMETERS OF LOWER LIMB SEGMENT

	Mass (% of weight)		Length (% of height)		Center of mass (% of height)	
thigh	m_t	11.50	L_t	25.60	S_t	12.80
crus	m_c	4.44	L_c	23.77	S_c	11.13
foot	m_f	1.90	L_f	11.75	S_f	5.12

In addition to the passive torque, physical joint also produces active torque ($\tau_h|_{active}$, $\tau_k|_{active}$, $\tau_a|_{active}$) by effort of muscle contraction. The effort of muscle contraction can be quantified by the electromyographic (EMG) signals. By constructing the connection between EMG signals and active torques, we can achieve the intent recognition. According to Rainoldi's study [18], we choose nine channels of EMG with good quality to be recorded, respectively from tensor fascia lata, rectus femoris, vastus lateralis, vastus medialis, biceps femoris, semitendinosus, gastrocnemius lateralis, gastrocnemius medialis, tibialis anterior. Eq.(10) indicates the raw EMG signals are processed with the Root Mean Square (RMS). The intent recognition is implemented with a feedforward neural network.

$$CHi_{RMS} = \sqrt{\frac{1}{N}\sum_{1}^{N} v_t^2} \tag{10}$$

To achieve the load and passive compensation and the EMG-based active control, the actuating torques of the exoskeleton should cover other torques including the load torques, the passive torques and the active torques, as expressed by Eq.(11). The total torques of lower limb joints (Eq.(12)) are the resultant torques of active torques, exoskeleton torques, passive torques and load torques. It can be seen that the total torques are larger than the active torques and

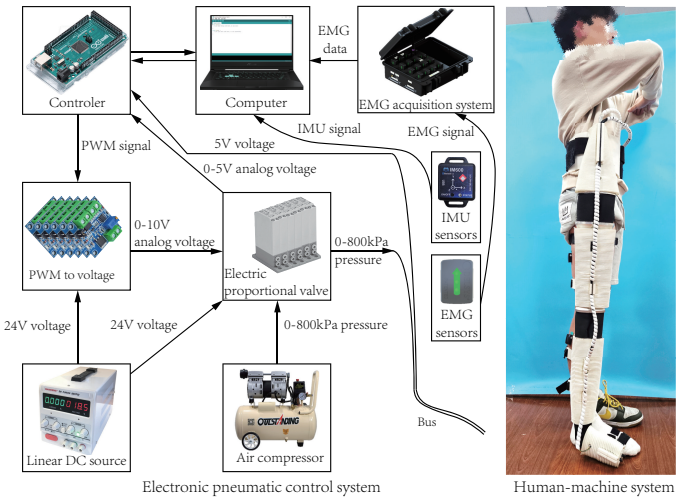

Fig. 5. Experimental platform and data flow of the exoskeleton robot.

are independent of the load and passive torques. The effort coefficient is the ratio of active torques with respect to total torques, which indicates the movement difficulty of human body. Increasing the assistance of exoskeleton (i.e. larger c_{assist}) reduces the movement difficulty of human body (i.e. smaller c_{effort}).

$$\tau|_{exosk} = \tau|_{load} + \tau|_{passive} + c_{assist}\tau|_{active} \tag{11}$$

where c_{assist} denotes the assistance coefficient of the exoskeleton.

$$\begin{aligned} \tau_{total} &= \tau_{active} + \tau_{exosk} - \tau_{passive} - \tau_{load} \\ &= (1 + c_{assist})\tau|_{active} \end{aligned} \tag{12}$$

$$c_{effort} = \frac{\tau_{active}}{\tau_{total}} = \frac{1}{1 + c_{assist}} \tag{13}$$

where c_{effort} denotes the effort coefficient of lower limb of human body.

The final step is to achieve torque control of the exoskeleton. Without torque sensors, the actual exoskeleton joint torque (τ) is estimated with the inflating pressure (P) and joint angle (θ) according to the characteristic equation of CPAM (Eq.(1)). The difference ($\Delta\tau$) between the target and actual torques is used to produce the inflating pressure (P) through a Proportional-Integral (PI) controller, expressed by Eq.(14). P is divided into two pressures (P_1, P_2) respectively for the left and right chambers of the actuator, expressed by Eq.(15). P_1, P_2 are finally implemented by the proportional valves.

$$P = K_P\Delta\tau + K_I\int \Delta\tau dt \tag{14}$$

$$\begin{cases} P_1 = \max(P, 0) \\ P_2 = \min(P, 0) \end{cases} \tag{15}$$

IV. Result

The experimental platform of the exoskeleton robot are shown in Fig.5. The platform includes electronic pneumatic control systenm and human-machine system. Computer receives human EMG signals from the EMG acquisition system (Trigno, 4kHz, DELSYS INC., USA), connects to the the control board (Arduino Mega 2560), sends instructions and receives signals. IMUs (IM948, 0.5-250Hz, Chenyi Co. Ltd, China) obtain angle information for feedback control. Control board connects to PWM to voltage moduels to control electric proportional valves (ITV0030-2BL, SMC) to provide a certain air pressure for the exoskeleton. The electric proportional valves provide pressure feedback to Arduino. The whole electronic system is powered by the personal computer and a linear DC source (MS-1203DS, Maisheng Co. Ltd., China), and the pressure of pneumatic system is supplied by an air compressor (800W-40L, OUTSTANDING, China). Since the motion cycle of the exoskeleton is long, the sampling frequency of the sensors can meet the requirements.

A. No-load gait tracking

Feedforward-feedback hybrid control (Fig.3) is used in no-load gait tracking test. We control the exoskeleton to track a gait cycle, collected from a participant (aged 25, 180 cm, 70 kg). The gait pattern was recorded during the participant's walking motion.

The proposed exoskeleton can achieve the motion of all phases in the gait cycle, shown in Fig.6(a). The system's inflation pressure is within 200 kPa. The gait cycle time is elongated into 20 s in the experiment due to limit of the CPAM's response speed. According to Rehabilitation Medicine (Sixth Edition, People's Health Publishing House), during the rehabilitation treatment in the acute phase (1-2 weeks after the onset of stroke), it is necessary to perform slow exercise, so it can complete the required movement. According to Fig.6(b-d), the bending angles of the CPAMs can be controlled effectively. Compared with only using feedback control, using a control method that combines feedforward and feedback can significantly improve control accuracy. The maximum tracking errors of the hip, knee, and ankle joints are 1.0°, 1.4° and 1.0° (3.4%, 2.9%, and 4.7% of the ROM), better than our previous research: 5.9°, 7.4° and 1.7° (16%, 17%, and 10% of the ROM) [11]. Closed loop control combining feedforward and feedback can solve the problems of low precision and delayed response of soft exoskeleton.

Fig.5 shows that the exoskeleton conforms well with human body and provides assistance of multiple DOFs and considerable ROM for the wearer's lower limb in passive movement, which may find its application in rehabilitation.

B. Human intention control

We conduct experiments on the human-machine system use the human-in-the-loop control (Fig.4) and test the participant (aged 25, 180 cm, 70 kg) wearing the exoskeleton with pressure OFF and pressure ON. The participant mainly complete three motions: hip flexion, knee flexion, and ankle dorsiflexion. Nine EMG sensors are attached to the participant's leg to obtain the EMG signals of different muscles,

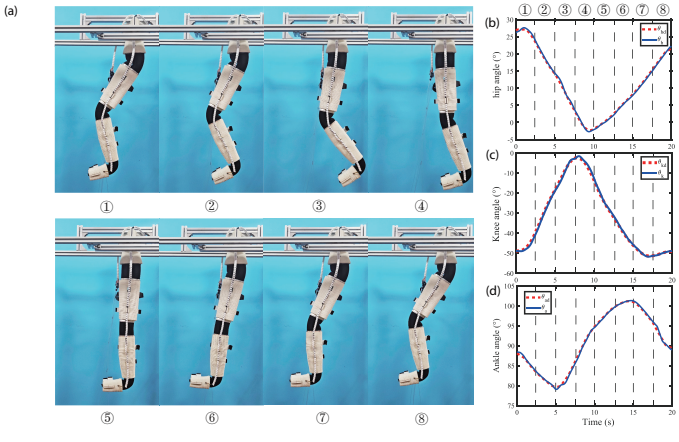

Fig. 6. The exoskeleton tracking the joint angles of a gait cycle. (a) The final states of different phases. (b–d) The joint angles, the dashed lines represent the reference signal, whereas the solid lines represent the actual signals. ① initial contact, ① to ② loading response, ② to ③ mid stance, ③ to ④ terminal stance, ④ to ⑤ preswing, ⑤ to ⑥ initial swing, ⑥ to ⑦ mid swing, ⑦ to ⑧ terminal swing.

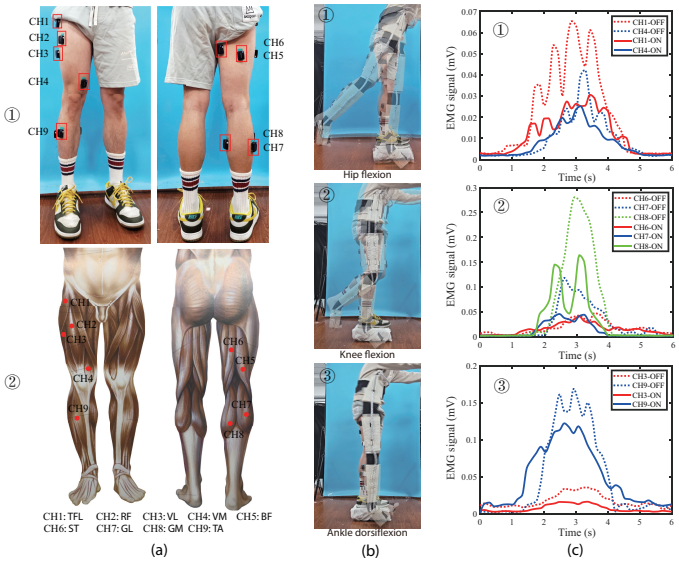

Fig. 7. The intentioin control. (a)Nine patch points of EMG sensors on ① participant body and ② human anatomy. (b) Three motions are actuated by multiple different characteristic muscle: ① hip flexion, ② knee flexion and ③ ankle dorsiflexion. (c) The EMG signals of the corresponding characteristic channels when human body completes three motions with exoskeleton pressure OFF/ON.

shown in Fig.7(a)①. The patch points are based on the positions of the corresponding muscles in human anatomy (Fig.7(a)②). The EMG signals are processed by bandpass filtering and root mean square (RMS). The three motions (Fig.7(b)) are actuated by multiple different characteristic muscle activations. CH1 and CH4 are more active during hip flexion. CH6, CH7, and CH8 are more active during knee flexion. CH3 and CH9 are more active during the ankle dorsiflexion. We call them characteristic channels.

In the experiment, when the exoskeleton is with pressure OFF, the participant actively completes three motions and moves to specified angles, and the EMG signals of the corresponding characteristic channel are recorded. When the exoskeleton is with pressure ON, the human-machine system recognizes the intention through the EMG signals of the corresponding characteristic channels, assists the participant to complete the corresponding actions, moves to the same angles, and records the EMG signals of the corresponding characteristic channels. The EMG signals are shown in Fig.7(c). The method of intention recognition is that the participant activates characteristic muscles, which can be recognized by the system, but is not enough to actuate body motions.

Experimental results show that the muscle activity of the condition with exoskeleton (pressure ON) is obviously lower the condition with exoskeleton (pressure OFF). Compared with the condition with exoskeleton (pressure OFF), its muscle activity decrease by 32.2% on average. The experiment has verified the effectiveness of exoskeleton Human-in-the-loop control. The user can control the bending angle of each joint of the exoskeleton through different muscle strengths, so that the exoskeleton produces a force-enhanced assist effect, and the level of assistance can be adjusted through coefficients and we w ill continue to conduct the human-in-the-loop control method in the future.

V. Conclusion

In this paper, we show a study on the design and control of a novel soft-rigid lower limb exoskeleton robot. First, based on anatomy, a novel exoskeleton structure design is proposed that applies Curl Pneumatic Artificial Muscles (CPAMs) to lower limb joints to actuate lower limb movement, and transmit force and motion through rigid parts. Second, a feedforward-feedback hybrid control method based on four CPAM characteristic models is proposed to improve the control accuracy and stability of the exoskeleton. Third, a human-in-the-loop control method based on human-robot hybrid dynamics modeling and human intentions and states is proposed to improve the human-robot interaction performance of exoskeletons. Experimental results show that feedforward-feedback hybrid control can reduce the maximum tracking error of the exoskeleton to 3.4% for hip, 2.9% for knee, and 4.7% for ankle joint. The exoskeleton can achieve intentional control based on EMG signals. With the assistance of the exoskeleton, the muscle activity of the human lower limbs is reduced by an average of 32.2%. The proposed soft-rigid lower limb exoskeleton robot has the advantages of being lightweight (weighs 5 kg, <14 kg [19], <6.5 kg [20]), having good flexibility, being comfortable wearing (stiffness $<0.13\,\mathrm{N\,m/^\circ}$, $<1.05\,\mathrm{N\,m/^\circ}$ [20], $<1.05\,\mathrm{N\,m/^\circ}$ [21]) and having good human-computer interaction, which can improve efficiency. In the future, the proposed soft-rigid lower limb exoskeleton robot will provide more effective intelligent rehabilitation equipment for patients with lower limb movement disorders.

References

[1] W. Liu, B. Yin, and B. Yan, "A survey on the exoskeleton rehabilitation robot for the lower limbs," in *2016 2nd international conference on control, automation and robotics (ICCAR)*. IEEE, 2016, pp. 90–94.

[2] W. Li, K. Liu, C. Li, Z. Sun, S. Liu, and J. Gu, "Development and evaluation of a wearable lower limb rehabilitation robot," *Journal of Bionic Engineering*, vol. 19, no. 3, pp. 688–699, 2022.
[3] D. Xu, Q. Wu, and Y. Zhu, "Development of a soft cable-driven hand exoskeleton for assisted rehabilitation training," *Industrial Robot: the international journal of robotics research and application*, vol. 48, no. 2, pp. 189–198, 2021.
[4] C. G. Rose and M. K. O'Malley, "Hybrid rigid-soft hand exoskeleton to assist functional dexterity," *IEEE Robotics and Automation Letters*, vol. 4, no. 1, pp. 73–80, 2018.
[5] H. Majidi Fard Vatan, S. Nefti-Meziani, S. Davis, Z. Saffari, and H. El-Hussieny, "A review: A comprehensive review of soft and rigid wearable rehabilitation and assistive devices with a focus on the shoulder joint," *Journal of Intelligent & Robotic Systems*, vol. 102, pp. 1–24, 2021.
[6] S. A. Dalley, C. Hartigan, C. Kandilakis, and R. J. Farris, "Increased walking speed and speed control in exoskeleton enabled gait," in *2018 7th IEEE International Conference on Biomedical Robotics and Biomechatronics (Biorob)*. IEEE, 2018, pp. 689–694.
[7] D. Sanz-Merodio, G. Puyuelo, A. Ganguly, E. Garces, A. Goñi, and E. Garcia, "Exotrainer project clinical evaluation of gait training with exoskeleton in children with spinal muscular atrophy," *Advances in Robotics Research: From Lab to Market: ECHORD++: Robotic Science Supporting Innovation*, pp. 211–227, 2020.
[8] T. M. Miller-Jackson, R. F. Natividad, D. Y. L. Lim, L. Hernandez-Barraza, J. W. Ambrose, and R. C.-H. Yeow, "A wearable soft robotic exoskeleton for hip flexion rehabilitation," *Frontiers in Robotics and AI*, vol. 9, p. 835237, 2022.
[9] Q. Liu, J. Zuo, C. Zhu, W. Meng, Q. Ai, and S. Q. Xie, "Design and hierarchical force-position control of redundant pneumatic muscles-cable-driven ankle rehabilitation robot," *IEEE Robotics and Automation Letters*, vol. 7, no. 1, pp. 502–509, 2021.
[10] L. Ma, Y. Leng, W. Jiang, Y. Qian, and C. Fu, "Design an underactuated soft exoskeleton to sequentially provide knee extension and ankle plantarflexion assistance," *IEEE Robotics and Automation Letters*, vol. 7, no. 1, pp. 271–278, 2021.
[11] J. Wang, Y. Fei, and W. Chen, "Integration, sensing, and control of a modular soft-rigid pneumatic lower limb exoskeleton," *Soft robotics*, vol. 7, no. 2, pp. 140–154, 2020.
[12] J. Wang, Z. Liu, and Y. Fei, "Design and testing of a soft rehabilitation glove integrating finger and wrist function," *Journal of Mechanisms and Robotics*, vol. 11, no. 1, p. 011015, 2019.
[13] Y. Wang, S. Yuan, M. Hou, X. Cui, S. Zhou, and Y. Fei, "Design, modeling and optimization of a high torque asymmetric dual chamber soft actuator," *Sensors and Actuators A: Physical*, p. 115635, 2024.
[14] J. Wang, Y. Wang, Y. Fei, and W. Chen, "Pneumatic bending soft actuator coupling with revolute joint with different boundary constraints," *IEEE/ASME Transactions on Mechatronics*, 2022.
[15] R. Riener and T. Edrich, "Identification of passive elastic joint moments in the lower extremities," *Journal of biomechanics*, vol. 32, no. 5, pp. 539–544, 1999.
[16] Y. Wang, Y. Li, J. Wang, Y. Fei, and J. Wan, "A novel high-torque bidirectional curl pneumatic muscle with stretchable sheath: Design and finite element method analysis," *IEEE Robotics & Automation Magazine*, 2023.
[17] F. Haugen, "The good gain method for simple experimental tuning of pi controllers," 2012.
[18] A. Rainoldi, G. Melchiorri, and I. Caruso, "A method for positioning electrodes during surface emg recordings in lower limb muscles," *Journal of neuroscience methods*, vol. 134, no. 1, pp. 37–43, 2004.
[19] S. Wang, L. Wang, C. Meijneke, E. Van Asseldonk, T. Hoellinger, G. Cheron, Y. Ivanenko, V. La Scaleia, F. Sylos-Labini, M. Molinari *et al.*, "Design and control of the mindwalker exoskeleton," *IEEE transactions on neural systems and rehabilitation engineering*, vol. 23, no. 2, pp. 277–286, 2014.
[20] K. Junius, B. Brackx, V. Grosu, H. Cuypers, J. Geeroms, M. Moltedo, B. Vanderborght, and D. Lefeber, "Mechatronic design of a sit-to-stance exoskeleton," in *5th IEEE RAS/EMBS International Conference on Biomedical Robotics and Biomechatronics*. IEEE, 2014, pp. 945–950.
[21] Y. Zhu, Q. Wu, B. Chen, and Z. Zhao, "Design and voluntary control of variable stiffness exoskeleton based on semg driven model," *IEEE Robotics and Automation Letters*, vol. 7, no. 2, pp. 5787–5794, 2022.